Journal of Molecular Structure 1099 (2015) 502–509

Contents lists available at ScienceDirect

Journal of Molecular Structure

journal homepage: http://www.elsevier.com/locate/molstruc

Synthesis and structural analysis of Co-doped $BaTiO_3$

L. Padilla-Campos [a, *], D.E. Diaz-Droguett [b], R. Lavín [c, e], S. Fuentes [d, e, **]

[a] Departamento de Química, Facultad de Ciencias Básicas, Universidad de Antofagasta, Casilla 170, Antofagasta, Chile
[b] Instituto de Física, Facultad de Física, Pontificia Universidad Católica de Chile, Casilla 306, Santiago, Chile
[c] Instituto de Ciencias Básicas, Facultad de Ingeniería, Universidad Diego Portales, Santiago, Chile
[d] Departamento de Ciencias Farmacéuticas, Facultad de Ciencias, Universidad Católica del Norte, Casilla 1280, Antofagasta, Chile
[e] Centre for the Development of Nanoscience and Nanotechnology, CEDENNA, Santiago, Chile

ARTICLE INFO

Article history:
Received 24 March 2015
Received in revised form
6 July 2015
Accepted 7 July 2015
Available online 10 July 2015

Keywords:
Barium titanate
Co-doped
Sol–gel processes
Structural properties
Theoretical calculations

ABSTRACT

$BaTiO_3$ doped with various percentages of Co (1–5 mol%) was synthesized using a combined sol-gel-hydrothermal method. The structural characteristics of the compounds were investigated using X-ray diffraction and Raman spectroscopy. Surface chemical information and oxidation states were studied using X-ray photoelectron spectroscopy. The magnetic properties of the samples were studied using magnetization curves. In addition, quantum chemical calculations were performed to elucidate the electronic structure of the samples and to understand the possible substitution mechanisms during Co-doping. The results indicated that Co effectively endowed the $BaTiO_3$ structure with intrinsic magnetic properties, which decreased as the Co percentage increased. In addition, the increase in the Co mol% produced a gradual loss of the non-perovskite structure, leading to a decrease in the ferroelectric behaviour.

1. Introduction

Barium titanate ($BaTiO_3$) has a typical perovskite structure and is the best-known and widely used material for electric ceramics due to its excellent dielectric [1,2], piezoelectric [3] and ferroelectric [4,5] properties. Recently, investigations into the incorporation of impurities (i.e., transition metals) in the $BaTiO_3$ (BT) structure determined that this doping can induce ferromagnetic properties, which results in a multifunctional material. In an interesting theoretical study, Cr, Mn, Co, and Fe-doping of BT were predicted to be the most promising candidates for inducing ferromagnetic properties in the material [6]. Based on this study, several experimental studies synthesized and characterized the properties of metal-doped BT with a greater emphasis on the compounds doped with Fe and Co [7]. In general, doped compounds exhibit ferromagnetic behaviour at room temperature but with a strong diamagnetic or paramagnetic component [6], depending of the doping concentration and density of oxygen vacancies inside the BT structure. In the special case of the Co-doped BT compound, the observed ferromagnetism may not be intrinsic due to the possibility of the formation of a secondary phase, such as Co clustering. This secondary phase may exhibit ferromagnetic behaviour, masking the overall properties of the compound. Therefore, the intrinsic nature of magnetic properties of Co-doped $BaTiO_3$ (BTC) remains unclear [8]. However, based on experimental studies of the BTC system, the ferromagnetic behaviour was determined to be strongly dependent on the synthesis method [8]. Several methods have been used for the synthesis of BTC, such as solid-state reactions [9], laser ablation [10], implantation [11], wet chemical processes [12] and hydrothermal methods [6]. The hydrothermal method is advantageous due to its low cost and low temperature of preparation, which results in good uniformity in the nanoparticle size [6,13–15].

The goal of the current study is to determine the structural, chemical, electronic and magnetic properties of BT compounds doped with different percentages of Co. The samples were synthesized using a combined sol-gel-hydrothermal method. In addition, the experimental results will be compared with theoretical results from quantum chemical calculations.

* Corresponding author. Departamento de Química, Facultad de Ciencias Básicas, Universidad de Antofagasta, Casilla 170, Antofagasta, Chile.
** Corresponding author. Departamento de Ciencias Farmacéuticas, Facultad de Ciencias, Universidad Católica del Norte, Casilla 1280, Antofagasta, Chile.
E-mail addresses: luis.padilla@uantof.cl (L. Padilla-Campos), sfuentes@ucn.cl (S. Fuentes).

http://dx.doi.org/10.1016/j.molstruc.2015.07.012
0022-2860/

2. Experiments

2.1. Synthesis

$BaTi_{1-x}O_3$:Co_x powders with x = 0, 1, 3 and 5 mol% Co were synthesised by the sol–gel hydrothermal process using tetrabutyl titanate (TBT), chloride barium ($BaCl_2$) and cobalt chloride ($CoCl_2$) as starting materials.

In a typical procedure, solution (A) containing 1 mL of TBT (97%) was diluted with 8.2 mL of ethanol for 10 min to form a white solution, which was added dropwise at 60 °C for 3 h with stirring to solution (B), which contained 1 ml of HNO_3 in 39 mL of deionised water (45 °C). Aqueous solution (C) was prepared by dissolving $BaCl_2 \cdot 2H_2O$ in 4 mL of deionised water, and solution (D) was prepared by dissolving $CoCl_2$ in 2 mL of deionised water.

To prepare the $BaTi_{1-x}O_3$:Co_x precursor, solutions (C) and (D) were added dropwise to solution (B). Under stirring and N_2 bubbling, KOH was added to the barium cobalt titanium solution to form a white homogeneous colloidal barium cobalt titanium slurry.

The mixed solution was transferred to a 500 mL Teflon-lined stainless steel reactor, sealed and heated to 180 °C for 24 h under an oxygen partial pressure of 14 bar. At the end of the reaction, the autoclave was cooled to room temperature. The as-synthesised white powder attached to the bottom and inner wall of the Teflon container was collected, centrifuged, washed with distilled water and ethanol to remove the remaining ions and dried at 60 °C for 6 h under reduced pressure.

2.2. Characterisation

X-ray diffraction spectra were acquired using a Siemens Advanced D-8 diffractometer with CuKα radiation at 40 kV and 30 mA. The Raman spectra were recorded on a WITEC model CRC200 using a 5.5 mW laser with a wavelength of 514.5 nm. The surface chemical information and oxidation states of the BTC samples were obtained from high-resolution X-ray photoelectron spectroscopy (XPS; Physical Electronics system model 1257) using Al Kα emission. The energy scale was calibrated by assigning 284.8 eV to the C 1s peak, corresponding to adventitious carbon. The magnetic properties were measured at room temperature (25 °C) using an alternating gradient magnetometer (AGM) MicroMag model 2900.

2.3. Theoretical details

To support the experimental results by providing the occupation site of Co in the $BaTiO_3$ structure (doped compound), we carried out quantum chemical calculations to determine the stability and electronic properties of this compound. To simulate the doped compound, cluster methodology [16–18] was employed where a finite number of atoms were used to represent the material, as shown in Fig. 1. The cluster consisted of eight unit cells. Two occupation sites were considered as follows: a) Co replacing Ti (Fig. 1a) and b) Co replacing Ba (Fig. 1b). In addition, to analyse the influence of the oxygen vacancies on the electronic properties of the doped compound, cluster models were designed and are shown in Fig. 1c and d. The energy and electronic properties were calculated by solving the Kohn–Sham equations in an atomic basis set formed by Gaussian functions. The calculations were performed using the B3LYP exchange correlation functional [19–22], which is a hybrid type of functional. This functional consists of careful mixing of Hartree–Fock exchange calculated with Kohn–Sham orbitals and B88 exchange functional [19] plus the LYP correlation functional [22]. For titanium and oxygen atoms, the 6-31G basis sets [23,24] were used. For the Ba and Co atoms, a pseudopotential from the Los Alamos group [25] with a corresponding basis set was employed. For calculational simplicity, the crystallographic data for cubic BT was employed to represent the doped compound [26,27]. Effective charges based on atomic polar tensors (APT) were used for discussion of the results [28]. All of calculations were performed using the Gaussian 09 program [29].

The energetic stability of the configurations with different Co occupation sites in the $BaTiO_3$ structure (Fig. 1) as well as the undoped compound was calculated as:

$$\Delta E = E(\text{system}) - E(\text{system} - X) - E(X) \quad (1)$$

where E(system) corresponds to the energy of the cluster model representing each of doped and undoped systems, E(system-X) corresponds to the energy of the doped with undoped system less a X atom (X = Ti, Ba or Co) and E(X) is the energy of a specific X atom.

3. Experimental results

3.1. X-ray diffraction

Fig. 2 shows the XRD patterns of the BT and BTC samples. As shown in Fig. 2, the sharp and well-defined peaks indicate highly crystalline nature of all of the as-prepared BTC powders, which were not subjected to any heat post-treatment. The XRD Bragg reflection was assigned to that of the cubic perovskite structure of BTC. In fact, all of the main peaks for the BTC samples, which are shown in Fig. 2, are apparently stabilised in the cubic lattice (space group *Pm3m*) for the BT powders at room temperature.

The inset in Fig. 2 shows the XRD patterns of BT and BTC in the 44–46° 2θ range. For the BT sample, splitting of the (2 0 0)/(0 0 2) diffraction peaks was observed, indicating that the sample was stabilized in the tetragonal phase or pseudo cubic phase with slight tetragonal distortion at room temperature. However, only a single diffraction peak was observed, and the effect of Co substitution on the BT structure shifts the (2 0 0) reflection, which is characteristic of the cubic lattice of BTC [8]. In addition, diffraction peaks corresponding to other phases were not observed. Therefore, the Co cluster was not formed.

The calculated values of lattice constants and due to higher ionic radius of the Co (0.9 Å for Co^{2+}) compared to that for Ti (0.605 Å for Ti^{4+}), expansion of the crystal lattice took place, increasing with the increase of Co concentration: 3.990 Å (BT), 4.0285 Å (BTC 1 mol%) and 4.0375 Å (BTC 3 mol%). However, this continuous shift in the XRD spectrum disappeared at BTC 5 mol%, as showed for the lattice constant value of 4.0205 Å. The latter result may be due to Co^{2+} ions replace both, Ba^{2+} and Ti^{4+}, producing a small lattice distortion that would explain the shift to lower 2θ values.

3.2. Raman spectroscopy

The Raman spectra obtained at room temperature for the synthesised BTC are shown in Fig. 3. The Raman spectra of the BTC samples are similar to those obtained for nanoparticles of pure BT in a previous study [30], and these spectra contain a characteristic Raman peak near 307 cm^{-1} (B1 mode) corresponding to the tetragonal BT phase, which contradicts the cubic symmetry observed by XRD analysis (BT) where no first-order Raman activity is expected. *Busca* et al. [31] reported a distortion of the TiO_6 octahedron in the cubic BT phase inducing pseudotetragonality of the cubic phase, which could explain the significantly lower symmetry with respect to the cubic perovskite structure that is similar to that of the tetragonal BT. In addition, in a previous structural analysis [15] of BT, a small displacement in the titanium atom along the Z-

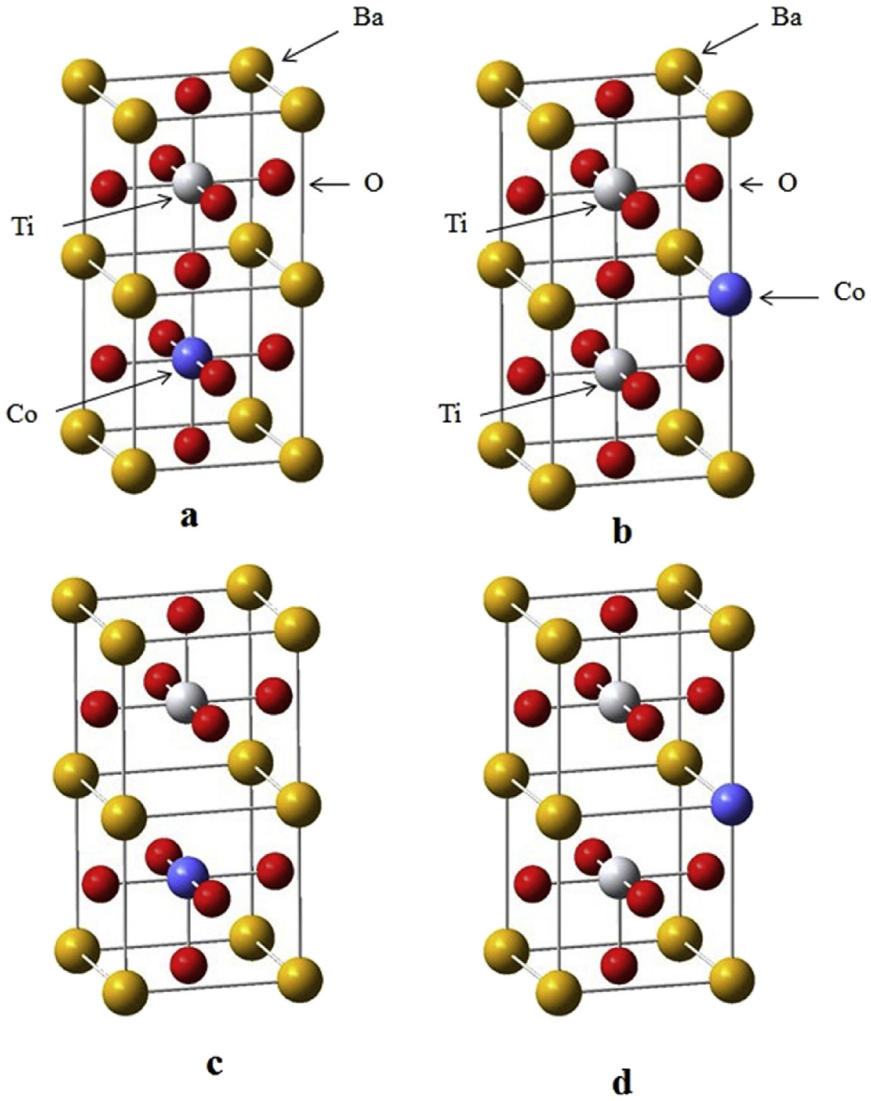

Fig. 1. Cluster model structures. a) Co replacing to Ti, b) Co replacing to Ba, c) and d) oxygen vacancies.

axis from ≥0.5 pm results in a pseudocubic or slightly tetragonal structure, which is in agreement with results reported by *Busca* et al. [31].

In general, for the BTC samples, four characteristic Raman bands were observed as follows: one band at approximately 307 cm^{-1} [B_1, E(TO+LO)], a broad band near 270 cm^{-1} [A_1(TO)], a band at approximately 519 cm^{-1} [A_1, E(TO)] and a band located at 720 cm^{-1} [A_1, E(LO)].

The cubic phase did not exhibit Raman active modes, and this polymorph typically exhibits broad bands at approximately 250 and 520 cm^{-1}, which may be due to local disorder associated with the positions of the Ti atoms. However, by increasing the Co concentration, the intensity of the Raman peaks changed. The bands associated with the tetragonal non-perovskite structure (307 cm^{-1}) decreased due to the tetragonal-to-cubic phase transition from BT to BTC. This result is in agreement with the effect observed from X-ray diffraction analysis where only the BT sample was stabilized in the tetragonal phase or pseudocubic phase with slightly tetragonal distortion.

The band at approximately 270 cm^{-1} exhibited a continuous increase but the band at approximately 520 cm^{-1} shifted to low frequencies (515 cm^{-1}). In addition, the intensity of the band decreased with the mol% of Co. The characteristic band at 720 cm^{-1} exhibited a minor relative intensity for BTC compared to that for BT, which may be due to defects, such as oxygen vacancies, in the BTC lattice [31].

Thus, the presence of band to 307 cm^{-1} was indicative of tetragonal phase of the BTC sample, i.e., conservation of ferroelectrical properties. However, tetragonality decreased with increasing of Co concentration and, gradual reduction of the ferroelectric behaviour could be expected.

3.3. X-ray photoelectron spectroscopy

Surface chemical characteristics and oxidation states of the constituent atoms of the BTC compound were obtained by XPS high-resolution measurements. A representative XPS spectrum of the BTC samples in the 802–773 eV energy range is shown in Fig. 4 for the 3 mol% Co-doped BT sample. The doublet was fitted using three curves. The binding energies (BEs) of 780.4 eV (Ba $3d_{5/2}$) and 795.7 eV (Ba $3d_{3/2}$) were attributed to Ba^{2+} ions in the non-perovskite structure (β) of the BT compound. The lowest BEs of 778.1 (Co $2p_{3/2}$) eV and 793.4 eV (Co $2p_{1/2}$) were associated with Co^{2+} ions. Finally, the intermediate peaks centred at 779.4 eV and

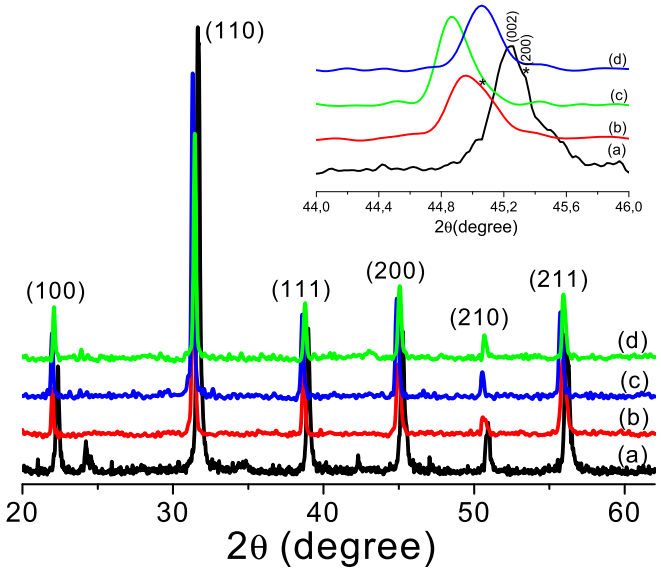

Fig. 2. XRD patterns of the BT nanoparticles doped with different content of Co: (a) 0%, (b) 1%, (c) 3% and (d) 5 mol%. The right side is the XRD patterns in the 2Θ region of 44 and 46.

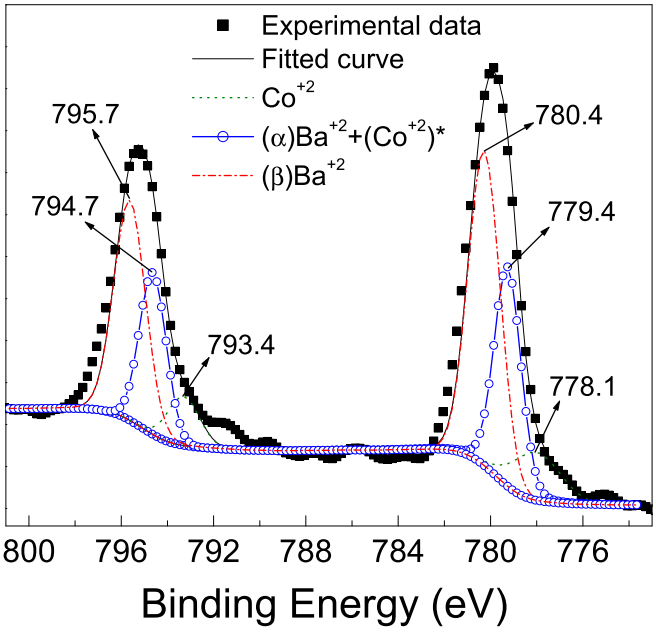

Fig. 4. High resolution XPS spectra of the 802–773 eV spectral range acquired from 3 mol% Co-doped BT sample.

794.7 eV are consistent with two overlapping photoelectronic signals. One signal was due to the presence of Ba^{2+} ions inside the perovskite structure (α) of the BT compound because their BEs are slightly lower than the ones corresponding to Ba^{2+} in the β-BT structure (non-perovskite). The energy difference is very small and typically less than 1.6 eV, as reported by *J. X. Liao* et al. [32] and *S. Nasser* et al. [33]. The second contribution to the peaks centred at 779.4 eV and 794.7 eV was attributed to the presence of Co^{2+} ions. However, these Co^{+2} experience a different chemical environment ($(Co^{2+})^*$) inside the BTC structure compared to the Co^{2+} ions with lower BEs values (778.1 eV and 793.4 eV).

Fig. 5a and b shows the fit obtained for the Ti 2p and O 1s XPS signals, respectively, from the 3 mol% Co-doped BT sample. The oxidation state changes of the O atoms are strongly associated with the oxidation state changes of the Ti atoms in the BT structure. The fit of the Ti 2p doublet (Fig. 5a) indicates that the titanium is primarily present as Ti4+ inside the BTC structure with BEs of 458.2 eV (Ti 2p3/2) and 464.0 eV (Ti 2p1/2). The presence of other oxidation states, such as Ti3+, was not detected when the spectrum was fit. The O 1s signal fit (Fig. 5b) required four curves. The BEs of 526.3 eV and 526.2 eV were attributed to O bound to Co^{2+} ions. The BEs of 528.1 eV and 527.7 eV were associated with the presence of oxygen bound to (α) Ba^{2+} and $(Co^{2+})^*$ ions. The 529.9 eV BE was associated with oxygen inside the non-perovskite BT structure with a $BaTi_{1-x}Co_xO_{3-x}$ stoichiometry, where x is the Co doping percentage. The highest binding energy was 531.8 eV, which was attributed to OH^- species chemisorbed on the BTC surface.

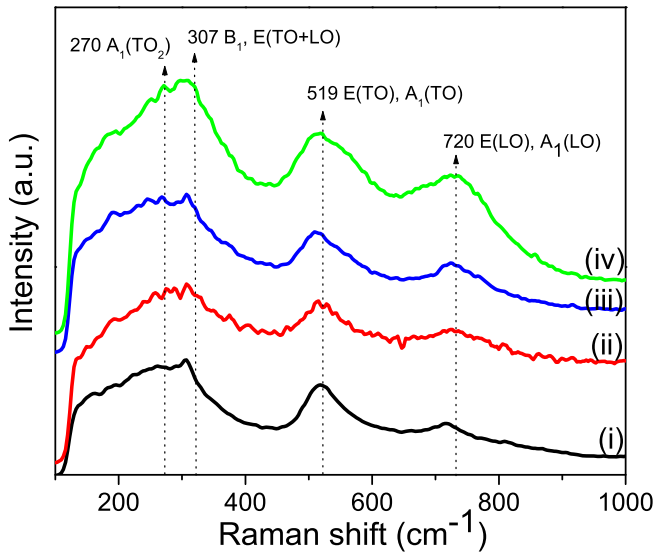

Fig. 3. Raman spectra for BT and BTC nanoparticles with doped with different content of Co: (i) 0%, (ii) 1%, (iii) 3% and (iv) 5 mol%.

3.4. Magnetic properties

The hysteresis curves measured at ambient temperature for the BTC samples are shown in Fig. 6. Table 1 lists the magnetic parameters that characterize the different doped samples. In general, all of the BTC samples with different Co concentrations exhibit ferromagnetic behaviour (i.e., non-linear magnetisation curves). The analysis of the hysteresis curves indicates that the Co-doping concentration modifies the magnetic properties of the samples including the high-field susceptibilities (χ_{hf}), coercivity (H_c), saturation magnetization (M_s) and remaining magnetization (M_r) (see Table 1). The samples with 3 and 5 mol% Co–doping exhibit a paramagnetic tendency due to positive χ_{hf} values. However, the sample with 1 mol% Co-doping exhibits a ferromagnetic tendency with significantly lower high-field susceptibility and negative which reveals a degree of ferrimagnetism in this sample. We also observed a clear relationship between the level of paramagnetism and coercivity in these samples. Therefore, when the high-field susceptibility was lower, the coercivity was higher. In addition, in the BTC samples with higher Co concentrations, the coercivity was lower, which results in a less ferromagnetic BTC compound. However, the opposite behaviour was observed for the saturation magnetization as a function of the Co concentration where a higher % Co produced a higher saturation magnetization. This behaviour may be due to the high percentage of Co in the sample inducing a

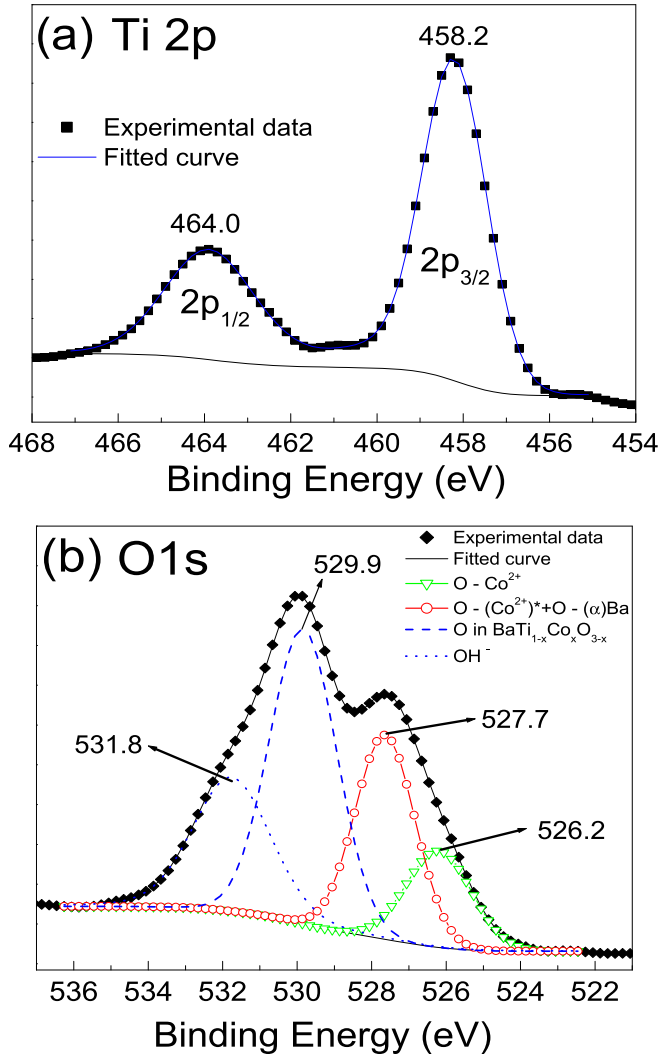

Fig. 5. Curve fitting results for (a) the Ti 2p signal and (b) O 1s signal from 3 mol% Co-doped BT sample.

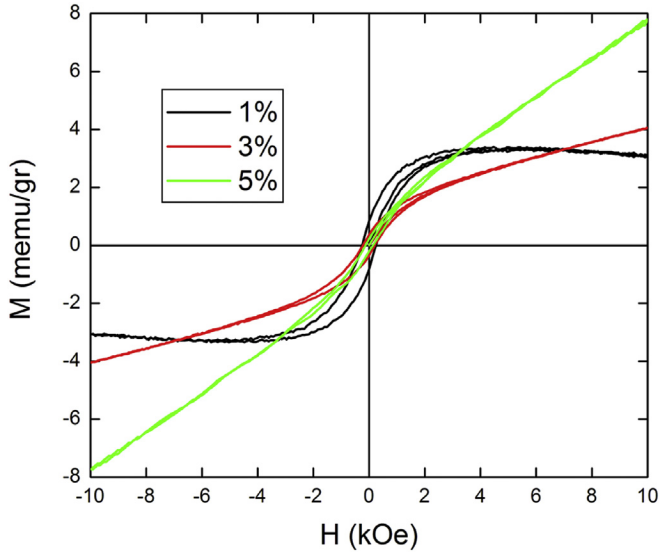

Fig. 6. Measured hysteresis cycles of the BT nanoparticles doped with different content of Co from 1% to 5 mol%.

Table 1
Magnetic properties of BTC samples.

% Co	*Ms*[memu/g]	*Mr* [μemu/g]	*Hc* [Oe]	χ_{hf}[m^3]
1	3.20	597.1	251.7	$-6.5e^{-15}$
3	3.94	506.1	212.8	$4.09e^{-14}$
5	8.07	290.6	134.4	$1.24e^{-13}$

higher magnetism in the material, which results in greater magnetization (M_S) in the BTC compound, as shown in Fig. 6 and Table 1.

3.5. Theoretical results

The effective charges and energetic stability of different compounds are listed in Table 2. The analysis of the effective charge indicated that when Co replaced Ti in the structure of BT, no variation in the oxidation state of the Ti atom was observed. However, when Co replaced Ba, a slight decrease in the oxidation state of the Ti atom and a slight increase in the oxidation state of the Co atom were observed. In both cases, the oxidation states of Ti and Co atoms are +4 and +2, respectively. Based on the energetic stability results, the replacement of Ti by Co is approximately twice as favourable as Co replacing Ba atoms. Therefore, the doping process was thermodynamically favoured by the first mechanism of substitution. To investigate if oxygen vacancies can induce changes in the oxidation state of elements that form the BTC structure, calculations using cluster models were performed, and the results are shown in Fig. 1c and d. The results indicated that oxygen vacancies do not induce significant changes in the oxidation state of the Co atom. The trend involves a slight increase in the oxidation state of Co as well as a decrease in the oxidation state of Ti by approximately 0.07e and 0.42e, respectively. However, oxygen vacancies produce a significant change in the oxidation state of Ti atoms, which would favour the presence of Ti^{3+}. However, this oxidation state was not observed in the XPS results. Co induces a decrease in the theoretical gap (energy difference between the valence band and the conduction band), where Co replaced Ba to produce a larger decrease (approximately 54%) compared to the replacement of Ti by Co, which only produce a decrease of 14%. Therefore, the replacement of Ti with Co replacing is more favourable for preserving the dielectric properties of the compound. In addition, when Co replaces Ti or Ba, an increase in the oxidation state of the O atoms (i.e., less negative charge) is observed, which is in agreement with the proposed stoichiometry of $BaTi_{1-x}Co_xO_{3-x}$ from the XPS results.

The densities of states for the undoped and doped structures are shown in Fig. 7. The percentage of elemental contribution is shown in Table 3. The analysis of the density of states indicates the following: a) In both doped structures, Co is present in the valence band (VB) and conduction band (CB) with a significant per cent of contribution, which is more than double that of Ba atoms. b) The replacement of Ti with Co primarily affects the contribution of O and Ba atoms in the VB. When Ba atoms are employed, only the Ba

Table 2
Effective charges (Q) and energetic stability (ΔE) for structures: a) undoped, b) Co replacing to Ti c) Co replacing to Ba.

Properties	a	b	c
Q(Ti)e	3.545	3.501	3.329
Q(O)e	−1.441	−1.351	−1.398
Q(Ba)e	1.390	1.359	1.387
Q(Co)e	–	1.448	1.629
ΔE(eV)	−24.42	−15.87	−7.43

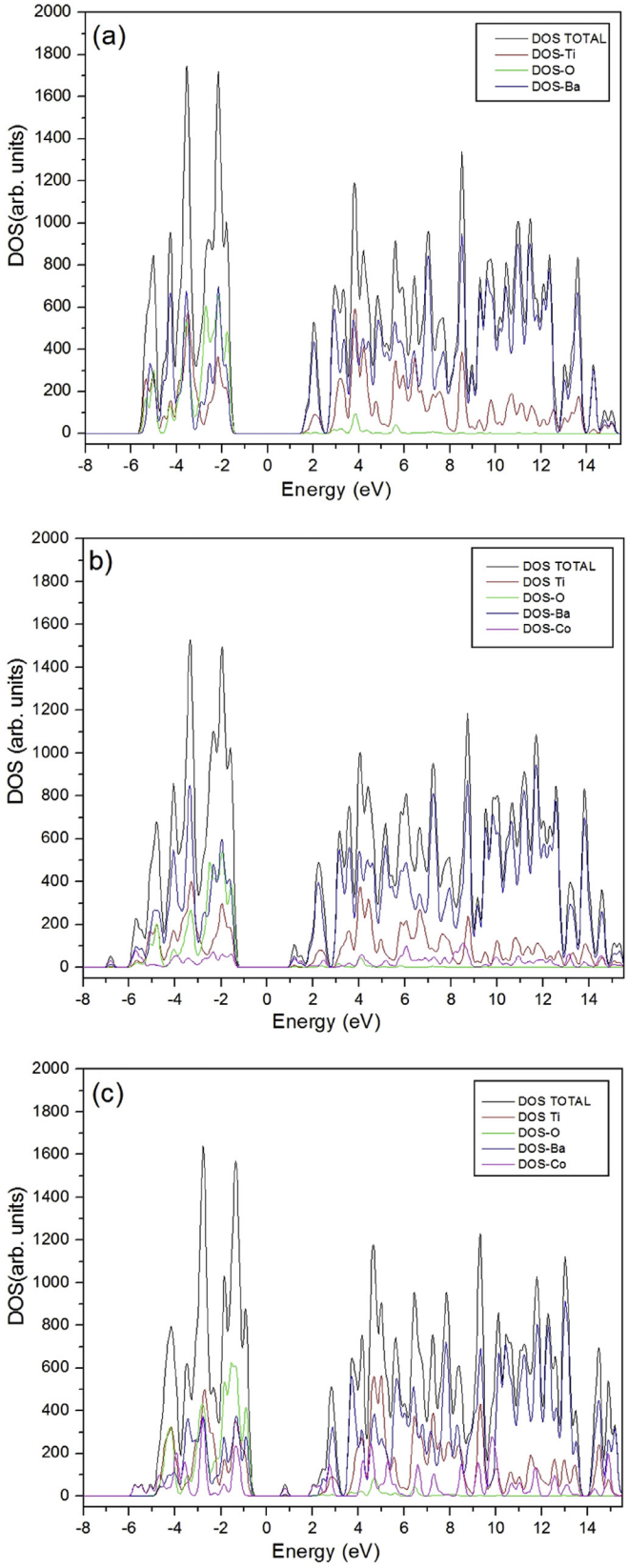

Fig. 7. Density of States for BT: a) undoped, b) Co replacing to Ti c) Co replacing to Ba.

atoms contribute to the VB. In the first case, a decrease and an increase in the contribution from the O and Ba atoms, respectively, were produced. In the second case, the contribution of Ba atoms decreased. c) In the CB, the replacement of Ti with Co primarily decreases the contribution to Ti atoms as well as the contribution of Ba atoms in compared to Co atoms.

Table 3
Percentage of elemental contribution to the density of states for $BaTiO_3$: a) undoped, b) Co replacing to Ti and c) Co replacing to Ba. Valence Band (VB) and Conduction Band (CB).

Element	a		b		c	
	VB	CB	VB	CB	VB	CB
Ti	27.1	31.3	22.1	23.3	27.0	33.7
O	36.5	2.8	26.9	1.5	35.1	3.2
Ba	36.4	65.9	45.5	70.5	25.2	49.4
Co	–	–	5.5	4.7	12.7	13.7

The partial contribution of d electrons from the Co atoms to the density of state for both doped structures is shown Fig. 8. A table with the percentage of contribution of spin is included in Fig. 8. The results indicate that independent of the occupying site, Co induces ferrimagnetic behaviour in the BT structure. However, this behaviour is more favourable when Co replaces Ti.

4. Summary and discussion

i) The XRD results indicate that the cubic phase was formed in the BTC samples. However, the peak asymmetry in the 44–46° 2θ range suggested some distortion in the structure of BT and BTC (1 mol%), which may be a tetragonal type of distortion. In addition, there was no evidence for the formation of a secondary phase. Therefore, the formation of a Co cluster was not observed, suggesting that the magnetic properties of BTC were intrinsic.

ii) The Raman results indicated that the tetragonal phase was formed in the BTC samples based on the band at 307 cm^{-1}, which indicated the presence of a tetragonal or pseudo cubic phase [15] that was in agreement with the results suggested by the XRD results (see above). We established in a previous study [15] that the Raman spectra are very sensitive to minor microstructural deformations, especially in the environment of the Ti positions in the BT lattice. These changes are not possible to detect using XRD. However, the tetragonal phase gradually converts to a cubic phase as the Co concentration increased, as shown in the Raman results. Thus, the presence of tetragonal phase in BTC samples was indicative of conservation of ferroelectrical properties. However, as tetragonality decreased with increasing of Co concentration, gradual reduction of the ferroelectric behaviour could be expected.

iii) For the Co-doped BT samples, the curve fitting XPS results for the 802–773 eV spectral range are difficult to interpret because the main doublet is the convolution result involves overlapped photoelectronic signals with very similar binding energy values. The binding energy difference of (β) Ba^{2+} and (α) Ba^{2+} was less to 1 eV (see Fig. 4). However, our assignment was supported by the XRD and Raman results that indicated the coexistence of a cubic phase (perovskite or α-phase) and a tetragonal phase (non-perovskite or β-phase). However, the tetragonality grade decreases as the Co doping percentage increases (see Fig. 3). The presence of Co^{3+}, which corresponds to a binding energy of approximately 780.0 eV [34,35], was ruled out in our XPS assignment because the simulation results revealed that the presence of Co^{2+} was energetically more favourable due to the substitution of Co atoms by Ti atoms during the doping. The presence of O vacancies that exhibit a signal in the same spectral range

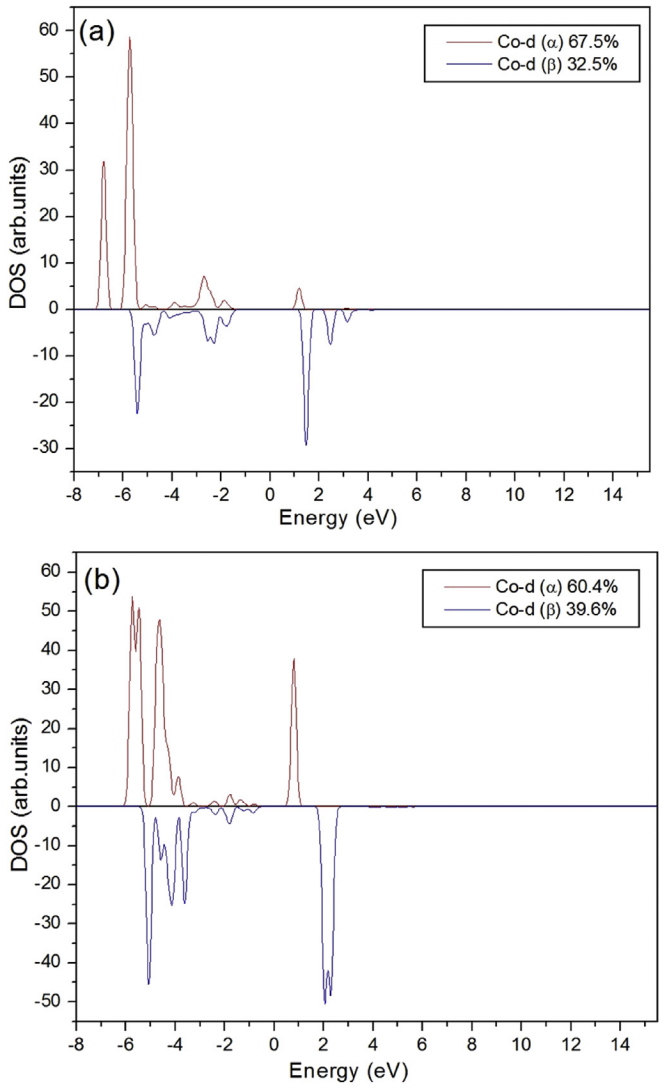

Fig. 8. Density of States of spin for d orbital of Co atom: (a) Co replacing to Ti and (b) Co replacing to Ba.

associated with OH^- species was also ruled out in the peak assignment shown in the Fig. 5b. If Ti^{4+} ions in the BTC structure were located near O vacancies, they could capture one electron decreasing their oxidation state to Ti^{3+} [36], which was not detected by the curve fitting of the Ti 2p signal (see Fig. 5a). In addition, the theoretical results confirming that the presence of Ti^{4+} in the BTC structure is energetically more favourable. All of the results indicate that the main substitution mechanism is Co^{2+} by Ti^{4+} atoms leading to a $BaTi_{1-x}Co_xO_{3-x}$ structure. Because the charge compensation cannot be due to the formation of O vacancies, a decrease in the electronic density of some O atoms inside the BTC structure may occur. This result is supported by the presence of different oxidation states of the O atoms (See Fig. 5b) and the presence of two types of Co^{2+} ions with different chemical environments (see Fig. 4).

iv) In general, the magnetic results indicated that the BTC samples exhibit a ferromagnetic behaviour. However, when the Co-doping concentration increased in the samples, the ferromagnetism decreases with a tendency toward an increases in the paramagnetic behaviour. The theoretical study of the doped system (BTC) indicated that the magnetic properties are more consistent with ferrimagnetic behaviour, which is more favourable when Co replaces Ti, result that is consistent with significantly lower high-field susceptibility and negative found for lower Co-doping concentration. In addition, from XPS result for higher Co-doping concentration, the probability that Co replaces to Ba is greater, and consequently the BTC compound becomes more paramagnetic, as is evidenced by a lower coercivity values.

v) The theoretical results indicated that Co in the BT structure perturbs the electronic properties of both the VB and BC. When Co replaces Ti in the BT lattice, the electronic properties of BT were not substantially affected, which preserves the dielectric properties. In contrast, when Co replaces Ba, a gap region in the BT structure and new electronic states near the VB were created. These results suggest that an increase in the Co-doping concentration produces an increase the probability that Co replaces Ba, which increases the paramagnetic behaviour of the BTC compound and decreases the dielectric properties due to a decrease in the theoretical gap. These results may explain the magnetic behaviour due to the Co concentration. The ferromagnetism decreases as the Co concentration increases.

5. Concluding remarks

BT samples doped with concentrations ranging from 1 to 5 mol% of Co (BTC samples) were synthesized by a sol–gel hydrothermal process, and the electronic and structural analyses were performed. The analyses of the structure of the BTC methods by different methods as well as the results from theoretical calculations were consistent with intrinsic magnetic properties that decrease with an increasing Co percentage. The improved properties of the BTC samples were predicted when Co replaces Ti, which preserves dielectric properties in BT and the magnetic properties in the BTC samples. However, the theoretical calculations supported the interpretation of the XPS spectra, especially the assignments of the peaks in the 802–773 eV energy range as well as the oxidation states of Co when incorporated into the BTC structure. Finally, all of the results were consistent with a $BaTi_{1-x}Co_xO_{3-x}$ stoichiometry for the most stable compound.

Acknowledgements

This work has been partially financed by FONDECYT grant under contract No 1110555, the basal Financing program CONICYT FB0807 (CEDENNA). D.E. Diaz-Droguett gratefully acknowledge to Fondecyt grant under contract No 11130555. Finally, the authors thank to Professor Jaime Llanos from Chemistry Department of Universidad Católica del Norte of Chile for stimulating discussion of some aspects of this paper.

References

[1] G.B. Li, S.X. Liu, F.H. Liao, S.J. Tian, X.P. Jing, J.H. Lin, Y. Uesu, K. Kohn, K. Saitoh, M. Terauchi, N. Di, Z.J. Cheng, The structural and electric properties of the perovskite system $BaTiO_3$–$Ba(Fe_{1/2}Ta_{1/2})O_3$, Solid State Chem. 177 (2004) 1695–1703.

[2] J. Xu, J. Zhai, X.J. Yao, Structure and dielectric nonlinear characteristics of $BaTiO_3$ thin films prepared by low temperature process, J. Alloys Compd. 467 (2009) 567–571.

[3] S. Sen, R.N. Choudhary, P. Pramanik, Synthesis and characterization of nanostructured ferroelectric compounds, Mater. Lett. 58 (2004) 3486–3490.

[4] Z. Wang, J. Hu, M. Yu, Axial polarization switching in ferroelectric $BaTiO_3$ nanowire, Nanotechnology 18 (2007), 235203–1-235203-4.

[5] J. Spanier, A. Kolpak, J. Urban, I. Grinberg, L. Ouyang, W. Yun, A. Rappe, H. Park, Ferroelectric phase transition in individual single-crystalline $BaTiO_3$

nanowires, Nano Lett. 6 (2006) 735–739.
[6] L. Yang, H. Qiu, L. Pan, Z. Guo, M. Xu, J. Yin, X. Zhao, Magnetic properties of BaTiO3 and $BaTi_{1-X}MxO_3$ (M=Co, Fe) nanocrystals by hydrothermal method, J. Mag. Mag. Mat. 350 (2014) 1–5.
[7] I.N. Apostolova, A.T. Apostolov, Safa Golrokh Bahoosh, Julia M. Wesselinowa, Origin of ferromagnetism in transition metal doped BaTiO3, J. Appl. Phys. 113 (2013), 203904–1-203904-4.
[8] H. Liu, B. Cao, C.J. O'Connor, Structural and magnetic properties o single-crystalline Co-doped barium titanate nanoparticles, J. Mag. Mag. Mat. 322 (2010) 790–793.
[9] S. Bagwan, M. Nagarbawadi, S.M. Rathod, V.V. Awati, D.H. Bobade, Solid state synthesis of niobium and Co-doped $BaTiO_3$, XRD, structural and enhanced dielectric properties of $BaTiO_3$, Int. J. Current Res. 5 (2013) 3149–3154.
[10] A. Ito, A. Machida, M. Obara, Cobalt doping in $BaTiO_3$ thin films by two-target pulsed KrF laser ablation with *in situ* laser annealing, Appl. Phys. Lett. 70 (1997) 3338.
[11] N.I. Khalitov, R.I. Khaibullin, V.F. Valeev, E.N. Dulov, N.G. Ivoilov, L.R. Tagirov, S. Kazan, A.G. Sale, F.A. Mikailzade, Structural and magnetic studies of Co and Fe implanted $BaTiO_3$ crystals, Nucl. Int. Meth. Phys. Res. B 272 (2012) 104–107.
[12] J. Wang, H. Zhang, Y. Li, Z. Li, Phase component and conductivities of Co-doped $BaTiO_3$ thermistors, J. Mater. Sci. Mater. Electron. 21 (2010) 811–816.
[13] S. Fuentes, F. Céspedes, L. Padilla-Campos, D.E. Diaz-Droguett, Chemical and structural analysis related to defects in nanocrystalline $Ba_{1-X}Sr_XTiO_3$ grown via hydrothermal sol–gel, Ceram. Int. 40 (2014) 4975–4984.
[14] S. Fuentes, E. Chávez, L. Padilla-Campos, D.E. Diaz-Droguett, Influence of reactant type on the Sr incorporation grade and structural characteristics of $Ba_{1-x}Sr_xTiO_3$ (x=0–1) grown by sol–gel-hydrothermal synthesis, Ceram. Int. 39 (2013) 8823–8831.
[15] E. Chávez, S. Fuentes, R.A. Zarate, L. Padilla-Campos, Structural analysis of nanocrystalline $BaTiO_3$, J. Molec. Struct. 984 (2010) 131–136.
[16] T.A. Kaplan, S.D. Mahanti, Electronic Properties of Solids Using Cluster Methods, Plenum Press, New York, 1995.
[17] L. Padilla-Campos, P. Fuentealba, Theoretical study of the adsorption of oxygen on a Cu(100) surface and the coadsorption with alkali atoms, Theor. Chem. Acc 110 (2003) 414–420.
[18] L. Padilla-Campos, E. Chavez, Electronic properties of small K_n ($n \leq 8$) and bimetallic K_nCu_m (n, $m \leq 4$) clusters, J. Molec. Struc. (THEOCHEM) 621 (2010) 92–100.
[19] A.D. Becke, Density – functional thermochemistry. III. The role of exact exchange, J. Chem. Phys. 98 (1993) 5648–5653.
[20] A.D. Becke, Density-functional exchange-energy approximation with correct asymptotic behavior, Phys. Rev. A 38 (1988) 3098–3100.
[21] B. Miehlich, A. Savin, H. Stoll, H. Preuss, Results obtained with the correlation energy density functionals of Becke and Lee, Yang and Parr, Chem. Phys. Lett. 157 (1989) 200–206.
[22] C. Lee, W. Yang, G.R. Parr, Development of the Colle–Salvetti correlation-energy formula into a functional of the electron density, Phys. Rev. B 37 (1988) 785–789.
[23] W.J. Hehre, R. Ditchfield, J.A. Pople, Self-consistent molecular orbital methods. XII. Further extensions of Gaussian-type basis sets for use in molecular orbital studies of organic molecules, J. Chem. Phys. 56 (1972) 2257–2261.
[24] V. Rassolov, J.A. Pople, M. Ratner, T.L. Windus, 6-31G* basis set for Third-Row Atoms, J. Chem. Phys. 109 (1998) 1223–1229.
[25] P.J. Hay, W.R. Wadt, Abinitio effective core potentials for molecular calculations. Potentials for the transition metal atoms Sc to Hg, J. Chem. Phys. 82 (1985) 270–284.
[26] H. Dittrich, N. Karl, S. Kück, H.W. Schock, Ternary Compounds, Organic Semiconductors, Springer-Verlag, U.S.A, 2000.
[27] P. Hermet, M. Veithen, P. Ghosez, Raman scattering intensities in $BaTiO_3$ and $PbTiO_3$ prototypical ferroelectrics from density functional theory, J. Phys. Condens. Matter 21 (2009), 215901–1-215901-10.
[28] J. Cioslowski, A new population analysis based on atomic polar tensor, J. Am. Chem. Soc. 111 (1989) 8333–8336.
[29] M.J. Frisch, G.W. Trucks, H.B. Schlegel, G.E. Scuseria, M.A. Robb, J.R. Cheeseman, G. Scalmani, V. Barone, B. Mennucci, G.A. Petersson, H. Nakatsuji, M. Caricato, X. Li, H.P. Hratchian, A.F. Izmaylov, J. Bloino, G. Zheng, J.L. Sonnenberg, M. Hada, M. Ehara, K. Toyota, R. Fukuda, J. Hasegawa, M. Ishida, T. Nakajima, Y. Honda, O. Kitao, H. Nakai, T. Vreven, J.A. Montgomery Jr., J.E. Peralta, F. Ogliaro, M. Bearpark, J.J. Heyd, E. Brothers, K.N. Kudin, V.N. Staroverov, T. Keith, R. Kobayashi, J. Normand, K. Raghavachari, A. Rendell, J.C. Burant, S.S. Iyengar, J. Tomasi, M. Cossi, N. Rega, J.M. Millam, M. Klene, J.E. Knox, J.B. Cross, V. Bakken, C. Adamo, J. Jaramillo, R. Gomperts, R.E. Stratmann, O. Yazyev, A.J. Austin, R. Cammi, C. Pomelli, J.W. Ochterski, R.L. Martin, K. Morokuma, V.G. Zakrzewski, G.A. Voth, P. Salvador, J.J. Dannenberg, S. Dapprich, A.D. Daniels, O. Farkas, J.B. Foresman, J.V. Ortiz, J. Cioslowski, D.J. Fox, Gaussian 09, Revision B.01, Gaussian, Inc., Wallingford CT, 2010.
[30] S. Fuentes, R.A. Zárate, E. Chávez, P. Muñoz, M. Ayala, R. Espinoza, Synthesis and characterization of $BaTiO_3$ nanoparticles in oxygen atmosphere, J. Alloys Compd. 505 (2010) 568–572.
[31] G. Busca, V. Buscaglia, M. Leoni, P. Nanni, Solid-state and surface spectroscopic characterization of $BaTiO_3$ fine powders, Chem. Mater. 6 (1994) 955–961.
[32] J.X. Liao, C.R. Yang, Z. Tian, H.G. Yang, L. Jin, The influence of post-annealing on the chemical structures and dielectric properties of the surface layer of $Ba_{0.6}Sr_{0.4}TiO_3$ films, J. Phys. D. Appl. Phys. 39 (2006) 2473–2479.
[33] S. Nasser, X-ray photoelectron spectroscopy study on the composition and structure of $BaTiO_3$ thin films deposited on silicon, Appl. Surf. Sci. 157 (2000) 14–22.
[34] C. Norman, C. Leach, In situ high temperature X-ray photoelectron spectroscopy study of barium strontium iron cobalt oxide, J. Membran. Sci. 382 (2011) 158–165.
[35] J. Jung, D. Edwards, X-ray photoelectron (XPS) and Diffuse Reflectance Infra Fourier Transformation (DRIFT) study of $Ba_{0.5}Sr_{0.5}CoxFe_{1-x}O_{3-\delta}$ (BSCF: x=0–0.8) ceramics, J. Solid. Stat. Chem. 184 (2011) 2238–2243.
[36] B. Zhang, Z. Quan, T. Zhang, T. Guo, S. Mo, Effect of oxygen gas and annealing treatment for magnetically enhanced reactive ion etched $(Ba_{0.65},Sr_{0.35})TiO_3$ thin films, J. Appl. Phys. 101 (2007) 014107–014115.